Raman spectroscopy of carbon nano-particles synthesized by laser ablation of graphite in water

J.F. Cardenas[a], T. Cadenbach[a], Z.-B. Zhang[b], C. Costa-Vera[a,c], A. Debut[d], A.V. Vaca[d], S.-L. Zhang[b], and J.L. Paz[a]
[a]*Departamento de Física, Escuela Politecnica Nacional,*
Apdo. 17-12-866, Ladron de Guevara E11-253, Edif. Ing. Civil Piso 1, EC 170109, Quito, Ecuador.
e-mail: cardenas9291@gmail.com
[b]*Institutionen för teknikvetenskaper, Fasta tillståndets elektronik,*
Ångströmlaboratoriet, Lägerhyddsvägen. 1, Box 534, 751 21 Uppsala, Sweden.
[c]*Grupo Ecuatoriano para el Estudio Experimental y Teórico de Nanosistemas (GETNano),*
Diego de Robles y Vía Interoceánica, USFQ, N104-E, Quito, Ecuador.
[d]*Centro de Nanociencia y Nanotecnología,*
Universidad de las Fuerzas Armadas ESPE, Sangolquí, Ecuador

Received 16 May 2016; accepted 4 November 2016

Carbon nanoparticles (CNPs) have been synthesized by laser ablation of polycrystalline graphite in water using a pulsed Nd:YAG laser (1064 nm) with a width of 8 ns. Structural and mesoscopic characterization of the CNPs in the supernatant by Raman spectroscopy provide evidence for the presence of mainly two ranges of particle sizes: 1-5 nm and 10-50 nm corresponding to amorphous carbon and graphite NPs, respectively. These results are corroborated by complementary characterization using atomic force microscopy (AFM) and transmission electron microscopy (TEM). In addition, large (10-100 μm) graphite particles removed from the surface are essentially unmodified (in structure and topology) by the laser as confirmed by Raman analysis.

Keywords: Raman spectroscopy; carbon nanoparticle; laser ablation; high resolution electron microscopy; atomic force microscopy.

PACS: 52; 78.30.-j

1. Introduction

Carbon exists in various possible forms, such as graphene, graphite, diamond, amorphous carbon and derivatives of these in the presence of other constituents, *e.g.* hydrogen, forming possibly hydrogenated amorphous carbon. Thus, researching on carbon materials is facilitated by using a technique that provides a unique finger-print for each of these phases. Further, to be appealing, a characterization tool must be non-destructive?, fast, with high lateral resolution and provide as much structural and electronic information as possible. All these requirements are embodied by Raman spectroscopy. Hence, Raman spectroscopy has been of distinguished importance in recent years when, *e.g.* investigating the electronic structure and optical properties of single walled carbon nanotubes [1] and graphene [2].

Synthesis of carbon nano-particles (CNPs) using different techniques has attracted increasing interest ever since the buckey-balls were discovered [3]. The synthesis of a range of different CNPs and their applications are the subject of research and development within a range of disciplines, such as biotechnology [4] and nanotechnology [5]. Presently, a particularly interesting technique for synthesizing high pressure phases is laser ablation in liquid (LAL) [6]. The laser beam induces a high temperature and a high pressure where the liquid provides the additional pressure gain compared to laser ablation in vacuum [7]. The high temperature of the ablated plume during laser ablation of graphite in water was confirmed by the work of Saito (2003) *et al* [8], where the plume temperature was determined to be between 4000-6000 K during the first 1000ns. Soon after LAL became known nanocrystalline diamond nano-particles (NCDNPs) were synthesized by LAL [9]. According to Yang's [10] theoretical predictions the range of sizes of NCDNPs are limited and depends on temperature and pressure. While several investigations have confirmed, by Raman spectroscopy and electron microscopy, the co-synthesis of NCDNPs and carbon allotrope NPs by LAL, using visible [11-13] and near-UV [14] nanosecond and near-infrared femtosecond [15] laser pulses, limited studies have so far investigated the distribution of grain size and its possible relation to carbon phases for CNPs formed by LA in water. Here, we show that Raman spectroscopy can provide detailed structural and mesoscopic information of the CNPs formed, which is not only a requirement to understand the complex process of LA (of graphite) in water but serves also to show the versatility and importance of the technique.

2. Material and Method

Laser ablation of CNPs was performed by irradiating a bulk polycrystalline graphite sample immersed in water and in sodium dodecyl sulfate (SDS) aqueous solution (1 weight %) using laser pulses with a width of 8 ns from a Nd:YAG laser (1064 nm). The laser pulse propagation direction was vertical with respect to the air/water surface, where the water level was normally about 3-5 mm above the graphite surface. Assuming a Gaussian beam profile, the characteristic waist

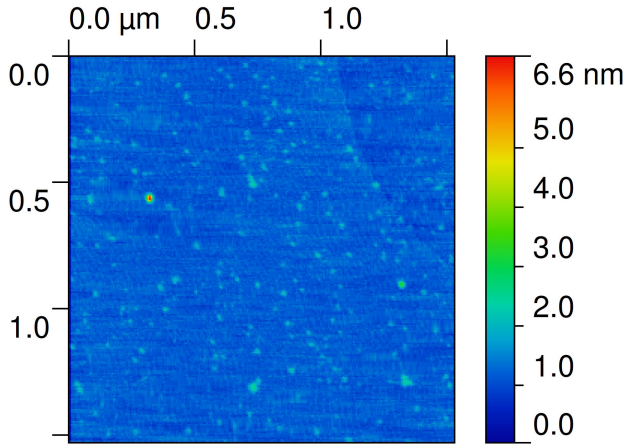

FIGURE 1. AFM image of CNPs (from the supernatant) on mica. Note that most particles are 1 nm heigh.

of the laser beam, σ, was estimated in the following way:a hole with a diameter of 0.1 mm was created in the glass slide by ablation using an energy, E_0, of about 150 mJ. Thus, since glass has a threshold ablation fluence, F_t, of $\sim$100 J/cm^2 [7,16], then r$_t$ (hole in glass $\sim$0.05 mm) is related to σ by $r_t^2 = -\sigma^2 \ln(F_t \pi \sigma^2 / E_0)$, yielding a $\sigma \sim 0.21$ mm. When performing ablation at the graphite/water interface the maximum fluence (peak fluence for a Gaussian distribution) was ~ 60 J/cm^2.

The CNPs were allowed to sediment for about 30 min before 10 μL of the top part of the dispersion (*i.e.* supernatant) was deposited on a mica substrate by spin coating (1200 rpm/min). In addition, an equal amount of the dispersion was deposited after the same time (as the spin coated) as well as after 24 hrs on mica and allowed to air dry. The drying took about 2 hrs. Thus, the samples represent different degrees of aggregation. Subsequently, the deposited CNPs on mica were characterized topographically using atomic force microscopy (AFM). When determining the height distribution of an image (Fig. 1) the following procedure was used: each pixel in Fig. 1 correspond to a value of the height relative to the average of the total distribution, which is zero $+-$ 3 nm. When dots with a height less than 3 nm is not excluded the distribution increases exponentially with decreasing height. Moreover, CNPs from the supernatant were deposited (2 hrs after synthesis) on a membrane for subsequent TEM and selected area electron diffraction (SAED) analysis.

Moreover, 1.5 ml of the supernatant (5 min after synthesis) were poured into a standard plastic cuvette (with a 1 cm trajectory) for subsequent standard light transmission measurements as a function of time after the LAL.

Furthermore, after having allowed the dispersion to sediment for about 2-4 hrs the sedimented CNPs and the supernatant were deposited onto optical glass slides for subsequent Raman spectroscopy analysis. Raman spectroscopy was performed using a Renishaw "InVia" spectrometer, a laser excitation wavelength of 532 nm, an objective of $\times$20 and approximately 0.3 mW at the sample spot. The fitting of the Raman bands was performed using Lorentzian functions for all peaks, where the peak ratios correspond to integrated intensity ratios (if nothing else is specified). Further, the raw spectra for the non-sedimented CNPs reveal a background, which increase with Raman shift and has been subtracted before peak fitting.

3. Results and discussion

As revealed in Fig. 1, most CNPs deposited on mica (spin coated sample) exhibit a height above the mica surface of the order of 1 nm, although there are some CNPs with heights on the order of 10-30 nm. Quantification of the AFM images reveals a shift of the height distribution towards larger particle heights in sequential order for the samples prepared by spin coating, air drying and air dried after 24 hrs aging. It should be mentioned that heights less than 3 nm are not incorporated in the analysis presented in Fig. 2, because quantification of the number of image pixels that represents real particles was difficult to perform for heights below 3 nm since noise is of the same order of magnitude. Despite this complication, it is possible to semi-quantitatively identify the range of heights for most particles. The second moment (variance) of the height distribution describes the width of the distribution and should increase with aggregation. Hence, the variances for the distributions associated with the spin coated, air dried and aged 24 hrs/air dried samples are 66, 77 and 119 nm^2, respectively. It is expected that particles will aggregate during the air drying process, thus the variance for the air dried sample is expected to be larger than for the spin coated sample. If, in addition, the carbon particles are allowed to aggregate for 24 hrs before being deposited on mica, and subsequently allowed to air dry, the particles will have a higher degree of aggregation and the variance is thus expected to be larger (as observed). Moreover, Fig. 3 shows a TEM image of CNPs deposited (2hrs after LA) on a membrane, which reveals an aggregate consisting of particles with sizes of about 20 nm surrounded by many smaller particles $\sim$5 nm corroborating qualitatively the findings of particle size distributions by

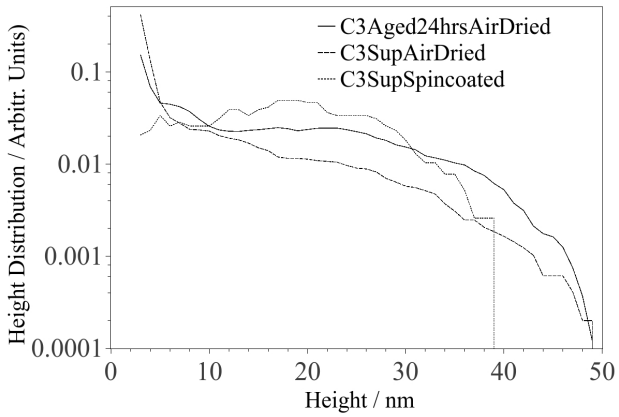

FIGURE 2. Height distributions of CNPs deposited on mica by spin coating, air drying and air drying after 24 hrs aging.

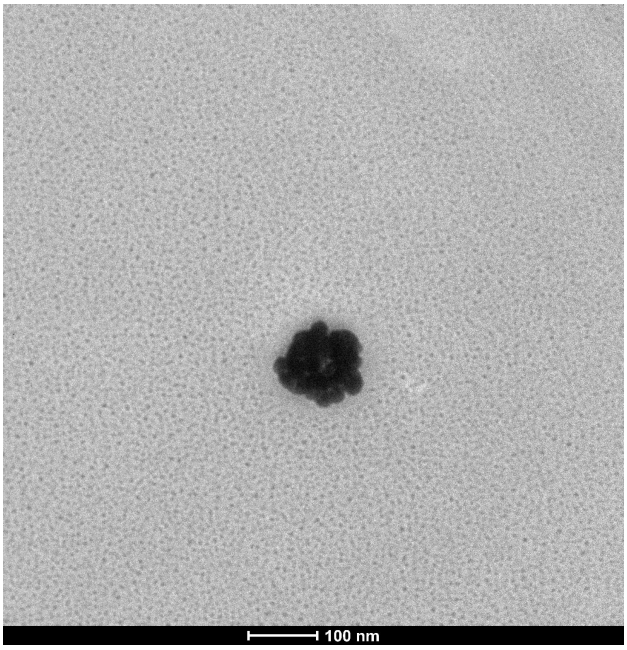

FIGURE 3. TEM image of the CNPs in the supernatant.

AFM (Fig. 1 and Fig. 2). Further, we are able to identify considerable sedimentation of particles already 5 min after the synthesis, which indicates that ablation results in the removal of a considerable amount of particles from the bulk with a size between 10 and 100 μm.

Optical transmission measurements of the CNPs in water, Fig. 1 (supporting information), were performed for different times (after synthesis): 15 min, 45 min, 24 hrs and 5 days. A relatively rapid increase in transmission with time is observed over the whole range of wavelengths. Thus, we attribute the increase of transmission to aggregation of small particles into larger ones, which eventually undergoes sedimentation. Normally, the presence of surfactants delays or inhibits the aggregation of nano-particles, which also is the case for graphite [17], NCDNPs [18] and nano-horn [19] CNPs. Indeed, when synthesizing CNPs by LAL in the presence of SDS, the increase in transmission is delayed, Fig. 2 (supporting information), although eventually aggregation appears to occur (as confirmed also by sedimentation). The inability to inhibit aggregation and subsequent sedimentation could be due to the small particle sizes ($\sim$1 nm) and to a low adsorption efficiency of SDS on non-crystalline CNP surfaces.

TABLE I. Parameters of the three Lorentzian functions fitted to the G-band in Fig. 4.

Peak	Area ($\times$104)	Center [cm^{-1}]	FWHM [cm^{-1}]
D	2.81	1348	57
G_H	4.55	1579	22
G_L	3.14	1530	214

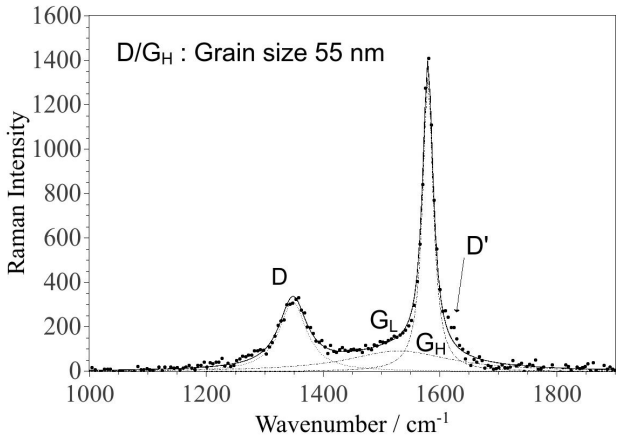

FIGURE 4. Raman spectrum of the sedimented CNPs deposited on glass. The fitting was performed using three Lorentzian functions. The parameters for each component are given in Table I.

The G-band (1500-1600 cm^{-1}) in the Raman spectra, is due to the presence of sp^2 carbon networks and the D-band ($\sim$1350 cm^{-1}) is due to the presence of sp^2 carbon in the form of rings, *i.e.* a structure that does not support π-electrons forming a ring (conjugated cyclic) system implies the absence of the D-band [20]. The spectrum for the CNPs sedimented after synthesis (Fig. 4) reveals mainly a G-band at 1579 cm^{-1} (G_H) with a FWHM of 22 cm^{-1} (Table I), which suggests a grain size of at least 10-20 nm [21]. In addition, the spectrum in Fig. 4 is consistent with a smaller but broader component, G_L, at 1530 cm^{-1}. Further, Fig. 4 reveals a D-peak at 1348 cm^{-1} and a D/G_H-ratio, which is well known to be inversely proportional to the grain size (the TK-relation [22], of $\sim$0.35 corresponding to a grain size of about 55 nm [23]. Note that this is the correlation length and corresponds to the length scale of the structural domains. Moreover, a certain fraction of the D-band is probably associated with the G_L-component, thus the D/G_L- ratio is an upper limit and consequently the grain size calculated is a lower limit. Hence, the large sedimented particles consist of grains of at least 55 nm in dimension. The presence of the disorder induced D'-peak at $\sim$1620 cm^{-1} has not been analyzed in detail but appears to scale with the size of the D-peak as expected [24].

The G-band of the particles in the supernatant (Fig. 5) is significantly different from the sedimented particles and is well fitted with two components with frequencies of 1535 and 1577 cm^{-1} (and a peak at $\sim$1609 cm^{-1}, which possibly is the disorder induced D'-peak) denoted as G_L and G_H, respectively. The significantly larger G_L component (compared to G_H) suggests a softening of the bonds (disordered sp^2-ring system), for which the TK-relation is no longer valid [22]. The high frequency component suggests either well graphitized (sp^2-rings) carbon or linear sp^2-chains (no D-band). From TEM and associated SAED images, the presence of faceted, Fig. 3 (supporting information) and Fig. 6, graphite with a size range between 20-50 nm is confirmed. Since graphite like particles in this size range (20-50 nm) are as-

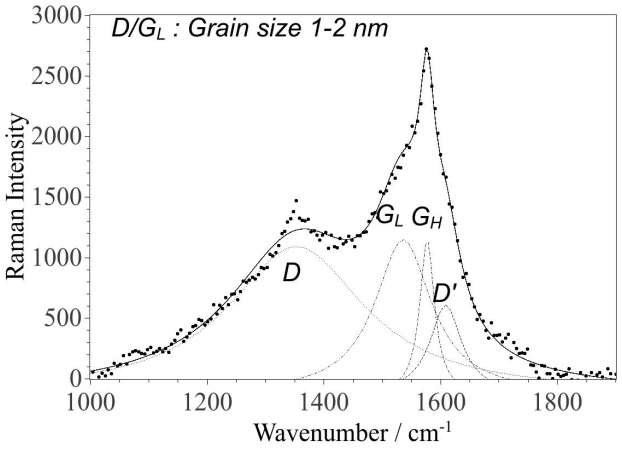

FIGURE 5. Raman spectrum of the CNPs from the supernatant deposited on glass. The fitting was performed using four Lorentzian functions. The parameters for each component are given in Table II.

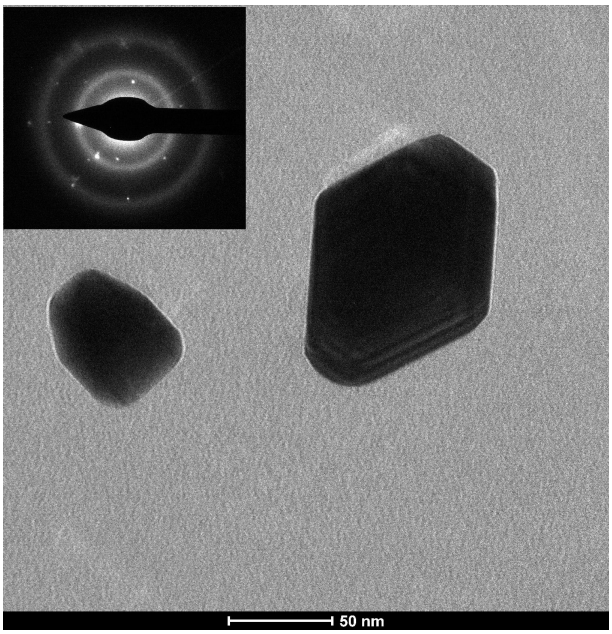

FIGURE 6. TEM image of a graphite CNPs from the supernatant. The inset depicts a SAED image from the large particle.

sociated with a D/G-ratio between 1 and 0.4 [23], the D-contribution from the G_H-component is negligible (maximum 25% of the total D-intensity). Thus, to a good approximation, since sp^2-chains do not give rise to a D-peak, we can assume that the D-band is only associated with the G_L-component which yields a D/G_L- ratio of 2.2. This corresponds to amorphous carbon with a structural domain size between 1 (if the peak intensity ratio is taken) and 2 nm [25]. Note, the absence of a characteristic Raman peak at 1333 cm^{-1} (associated with diamond) do not necessarily mean the absence of NCDNPs, since the Raman cross-section of diamond is about $\sim$100 times smaller than graphite when using visible excitation [21].

TABLE II. Parameters of the four Lorentzian functions fitted to the G-band in Fig. 5.

Peak	Area ($\times$104)	Center [cm^{-1}]	FWHM [cm^{-1}]
D	54.2	1353	284
G_L	23.5	1536	118
G_H	6.07	1577	30
D'	7.49	1609	65

TABLE III. Characteristic size parameter from data analysis of CNPs obtained by different methods for particles in the supernatant. Note that AFM do not reveal structure, although we have attributed the two particle ranges to different phases according to Raman and TEM observations.

Method	Size (nm) -amorphous carbon	Size (nm) -graphite
AFM	1 - 2	10 - 40
Raman (D/G-ratio)	1 - 2	
Raman (FWHM)	1 - 2	> 10
TEM	5	10 - 50

The FWHMs of the G_L and G_H components (Table II) suggest an sp^2 grain size of the order of 1-2 nm (in agreement with the D/G_L- ratio of 2.2) and at least 10 nm, respectively [21]. This analysis of the Raman spectrum (Fig. 5/Table II) is in good agreement with the AFM images (spin coated sample in Fig. 1 and Fig. 2) and the TEM images (Fig. 3, 6) for the particles in the supernatant, where most particles are in the 1-2 nm range (AFM) and 5 nm (TEM). This size range is in agreement with similar recent observations of LA of graphite in liquid [26]. Note that the TEM images suggests larger sizes, but the size ratio between the smaller and larger particles coincides with AFM and Raman observations, which could be explained if the particle shapes have a tendency of being oblate with their major faces oriented towards the supporting mica/membrane. The observed larger grain size associated with the G_H component correlates well with the height distribution of the deposited CNPs on mica (Fig. 2) and TEM images (Fig. 6), in particular for the spin coated sample. Hence, small particles (1-2 nm) consisting of amorphous sp^2-rings coexist with larger particles consisting mostly of graphite-like carbon and possibly some amount of carbon with sp^2-chain configuration with small D-band contribution. In Table III the characteristic particle size determinations, for CNPs in the supernatant, by the different methods are shown. It should be mentioned that the G-band varied slightly depending on where the incident laser spot (from the excitation laser) was positioned on the sample with particles from the supernatant, *i.e.* the relation between the four Lorentzian peaks varied slightly with position, which implies the presence of two or more phases among the non-

sedimented particles (consistent with the presence of both G_H and G_L components).

The formation of CNPs in water could possibly result in hydrogenation of amorphous carbon (a-c:H). The Raman bands for the CNPs in the supernatant reveal an increasing background (subtracted in Fig. 5) with Raman shift due to photoluminescence, which normally occurs for a-C:H. However, based on previous work on a-C:H [27], we conclude that the FWHM and peak-position for the components in Table II are not consistent with a-C:H (in any known form). Note that, luminescence has been observed from acid functionalized CNPs with a graphite-like structure [28]. Furthermore, evidence for a transition from normal vaporization to phase explosion has been obtained for laser ablation of several materials (including graphite in vacuum), showing a dramatic increase in the ablation rate at the threshold fluence of 22 J/cm^2 for graphite [29]. This suggests that the large particles that undergo sedimentation in the present work could be the result of phase explosion and the smaller particles a result of normal vaporization. However, further work is required to confirm this hypothesis.

4. Conclusions

Raman spectroscopy has been used to investigate CNPs synthesized by laser ablation of graphite in water. Large graphite-like particles of a size between 10 and 100 μm and with a grain size of the order of 55 nm, forms and undergo rapid sedimentation. Moreover, particles with sizes of the order of 1-5 nm and 10-50 nm with amorphous and graphite like structure remain in the supernatant, respectively. In addition, despite that LA of graphite is performed in water, Raman spectroscopy analysis indicates hydrogenated amorphous carbon do not form in a detectable amount. These results are important basic information for the understanding of the required physical conditions for the formation of a specific phase during laser ablation.

Acknowledgments

Authors, JFC, TC and JLP acknowledge the financial support provided by the Secretaría Nacional de Educación Superior, Ciencia, Tecnología e Innovación (SENESCYT) of Ecuador through the Prometeo Fellowship. Authors, SLZ and ZBZ acknowledge the financial support from the Knut and Alice Wallenberg Foundation (No. 2011.0082) and the Swedish Foundation for Strategic Research (SE13-0061). Further, access to the AFM instrument provided by Dr. Cristian Santacruz (EPN) is acknowledged.

1. M.S. Dresselhaus, G. Dresselhaus, A. Jorio, A.G. Souza Filho, R. Saito, *Carbon* **40** (2002) 2043.
2. A.C. Ferrari, D.M. Basko, *Nat. Nanotechnol.* **8** (2013), 235.
3. H.W. Kroto, J.R. Heath, S.C. O'Brien, R.F. Curl, R.E. Smalley, *Nat.* **318** (1985) 162.
4. C.R. Martin, P. Kohli, *Nat. Rev. Drug Discovery* **2** (2003) 29.
5. F. E. Kruis, H. Fissan, A. Peled, *J. Aerosol Sci.* **29** (1998) 511.
6. A.V. Simakin, V.V. Voronov, N.A. Kirichenko, G.A. Shafeev, *Appl. Phys. A* **79** (2004) 1127.
7. R. Fabbro, J. Fournier, P. Ballard, D. Devaux, J. Virmont, *J. Appl. Phys.* **68** (1990) 775.
8. K. Saito, *Prog. Mater. Sci.* **197-198** (2002) 56.
9. S.B. Ogale, A.P. Malshe, S.M. Kanetkar, S.T. Kshirsagar, *Solid State Commun.* **84** (1992) 371.
10. G.W. Yang, *Prog. Mater. Sci.* **52** (2007) 648.
11. L. Yang, P.W. May, L. Yin, J.A. Smith, K.N. Rosser, *Diamond Relat. Mater.* **16** (2007) 725.
12. G.-W. Yang, J.-B. Wang, Q.-X. Liu, *J. Phys.: Condens. Matter* **10** (1998) 7923.
13. S.R.J. Pearce *et al., Diamond Relat. Mater.* **13** (2004) 661.
14. D. Amans *et al., Diamond Relat. Mater.* **18** (2009) 177.
15. A. Santagata *et al., J. Phys. Chem. C* **115** (2011) 5160.
16. B.C. Stuart, M.D. Feit, S. Herman, A.M. Rubenchik, B.W. Shore, M.D. Perry, *J. Opt. Soc. Am. B* **13** (1996) 459.
17. J. Lu, I. Do, H. Fukushima, I. Lee, L. T. Drzal, *J. Nanomater.* **2010** (2010) 2:1.
18. F. Neugart *et al., Nano Lett.* **7** (2007) 3588.
19. M. Zhang, M. Yudasaka, J. Miyawaki, J. Fan, S. Iijima, *J. Phys. Chem. B* **109** (2005) 22201.
20. M.A. Pimenta, G. Dresselhaus, M.S. Dresselhaus, L.G. Cançado, A. Jorio, R. Saito, *Phys. Chem. Chem. Phys.* **9** (2007) 1276.
21. A. C. Ferrari, J. Robertson, *Philos. Trans. R. Soc., A* **362** (2004) 2477.
22. F. Tuinstra, J.L. Koenig, *J. Chem. Phys.* **53** (1970) 1126.
23. L.G. Cançado *et al., Appl. Phys. Lett.* **88** (2006) 163106.
24. P. Tan, Y. Deng, Q. Zhao, *Phys. Rev. B* **58** (1998) 5435.
25. A.C. Ferrari, J. Robertson, *Phys. Rev. B* **61** (2000) 14095.
26. X.D. Ren, R. Liu, L.M. Zheng, Y.P. Ren, Z.Z. Hu, H. He, *Appl. Phys. Lett.* **107** (2015) 141907.
27. C. Casiraghi, A.C. Ferrari, J. Robertson, *Phys. Rev. B* **72** (2005) 085401.
28. S.C. Ray, A. Saha, N.R. Jana, R. Sarkar, *J. Phys. Chem. C* **113** (2009) 18546.
29. N.M. Bulgakova, A.V. Bulgakov, *Appl. Phys. A* **73** (2001) 199.